MASS LOSS ALONG THE GIANT BRANCH OF THE GLOBULAR CLUSTER 47 TUC

A. Jorissen[1], **P.F. Coheur**[1], **R. Alvarez**[1], **M.A.T. Groenewegen**[2]
[1]Institut d'Astronomie et d'Astrophysique, Université Libre de Bruxelles, Belgium
[2]Max Planck Institut für Astrophysik, Garching bei München, Germany

ABSTRACT

Preliminary results are presented for the ISO guest observer program 47TUC aimed at deriving the mass loss rates of AGB and RGB stars of different luminosities in the galactic globular cluster 47 Tuc.

Raster maps of 5 fields covering areas of about $7 \times 7\,\mathrm{arcmin}^2$ at different distances from the center of the cluster have been obtained with ISOCAM at $11.5\,\mu$m (LW10). The present paper presents preliminary results for a field centered $6'$ East from the cluster center. No dust-enshrouded AGB stars have been found in that field. A sensitivity threshold of about 0.7 mJy is achieved, allowing to detect giant stars at $11.5\,\mu$m all the way down to the horizontal branch. Color indices combining ISO and DENIS data are derived in order to investigate the amount of dust emission (and hence mass loss rate) as a function of luminosity along the RGB and AGB. Dust shells are only detected around the Mira and semi-regular variable stars which populate the tip of the giant branch. This conclusion confirms the importance of stellar pulsations in the mass loss process.

Key words: globular cluster 47 Tuc; mass loss; AGB; DENIS; Mira variables.

1. OBSERVATIONS

ISOCAM mosaics of 5 fields at different distances from the center of the 47 Tuc cluster have been performed with the LW10 filter (closely matching the IRAS $12\,\mu$m filter). Only the eastern field (which has been observed with the Astronomical Observation Template parameters summarized in Table 1) will be discussed here. It is a 9×9 mosaic centered 6 arcmin east from the cluster center. Since the step size is half the chip size in both directions, the sources in the central region have 4 independent detections, with a total integration time of $4 \times 10 \times 2.1$ s per source, which provides a good compromise between detecting sources as faint as possible without saturating the brightest sources.

Table 1. Astronomical Observation Template parameters for the field 47 Tuc East

Field center (J2000)	0h25m30s $-72°05'$
Date of observation	JD 2450229.875
Filter	LW-10 (center $11.5\,\mu$m, range 8.0-$15.0\,\mu$m)
Detector gain	1
Pixel Field of View	$3''$ (large field mirror)
Number of pointings	9×9
Step between two pointings	$45''$ (1/2 chip size)
Total field size	$7.5' \times 7.5'$
$N_{\rm stab}$	30
$N_{\rm obs}$	10
$T_{\rm int}$ (s)	2.1

2. REDUCTIONS

2.1. ISOCAM Image

The reduction of our ISOCAM data poses a special challenge as we are aiming at extracting sources as faint as possible in a field containing very bright (AGB) sources. Because of the strong detector memory effects, these sources will leave ghost images in the next pointings that ought not to be confused with faint sources. The use of the PRETI routines allowed to overcome at least some of these problems. They were designed by Starck et al. (1998; see also Aussel et al. 1998) specifically for the detection of faint sources on ISOCAM images.

The main steps of the reduction process are as follows. The default dark frame is first subtracted from the raw data (CIER files) using the CAM Interactive Analysis (CIA) package. The bad column 23 is replaced by the average of columns 22 and 24. The cosmic rays are identified from their typical pattern in a multi-resolution median filter, and the affected readouts are masked. Remaining long-term drifts (mainly due to the detector memory effect after passing on bright sources, and to the change of the ISOCAM configuration at the beginning of the observation) are suppressed by subtracting the baseline of each pixel's time history (with all the individual images concatenated). The flat field is constructed from the median of the data themselves, since about 810 ($=10 \times 9 \times 9$) readouts are available per pixel. The detector tran-

Table 2. Comparison of IRAS and ISOCAM 12 μm fluxes (the latter should be considered preliminary; see Sect.3). IRAS fluxes are from Gillett et al. (1988), and K_0 magnitudes from Frogel et al. (1981). A zero-magnitude flux of 620 Jy at K has been adopted, following Beckwith et al. (1976).

Star	Alternate name	$F(12)$ (Jy)		K_0	$F(2)$ (Jy)	$F12/F2$	
		IRAS	ISOCAM			IRAS	ISOCAM
V3		0.215	0.206	6.0 – 6.5	1.56 – 2.47	0.09 – 0.14	0.08 – 0.13
V15	W300	0.041	0.041	7.26	0.77	0.05	0.05
V11	W12	–	0.100	6.68	1.32	–	0.08
V18	L168	–	0.101	7.44	0.66	–	0.15
V11+V18		0.235	0.201	–	1.98	0.12	0.10
V7		<0.02	0.053	6.96	1.02	<0.02	0.05

sient is corrected by assuming that the first readout corresponds to 60% of the stabilized signal. In the present analysis, the fluctuations arising on top of the bright sources (probably caused by the jitter of the satellite) are often confused with cosmics and unduly masked, resulting in a loss of useful readings for bright sources. This problem must be addressed in a future reduction process.

The individual mosaic frames are then coadded into a single image. The source detection is performed on that image (Fig. 1) using a wavelet transform, which detects at each scale all pixels of the image above a given threshold σ of the noise map (Starck et al. 1998). A good compromise between maximum sensitivity and minimum number of false detections (as compared to optical sources; see Section 2.3) is obtained with a detection threshold set at 3σ. The source fluxes are obtained by aperture photometry on the reduced image, with the background estimated from the median of the pixel values in an annulus circling the source. The measured ADU are converted to Jansky units using the conversion factor provided in the ISOCAM observer manual (v.1, 1994).

To check the reduction process, it is useful to compare the ISOCAM fluxes with previous results obtained by Gillett et al. (1988) from pointed IRAS observations of 47 Tuc (Table 2).

The 12 μm fluxes are in good agreement for the three stars in common to the two samples, the largest deviation (18%) being obtained for the composite source $V11 + V18$. The non-detection of $V7$ by Gillett et al. (1988) is surprising, since its flux at the time of our ISOCAM observation is similar to that of $V15$ which was detected by Gillett et al. (1988). This indicates that this star may be strongly variable at 12 μm. Since the faintest source detected by Gillett et al. (1988) has $F12 = 18$ mJy (in agreement with their $3\sigma = 12$ mJy detection threshold), $V7$ must have been fainter than about 20 mJy at the time of the Gillett et al. observation. This would imply a variability range of at least a factor of 2 at 12 μm for this star, since it had a flux of about 50 mJy at the time of the ISOCAM observation. A variability by a factor 2 at 12 μm is not uncommon among oxygen-rich Mira variables (Le Bertre 1993; Jorissen & Knapp 1998; Onaka et al., this conference). Fox (1982) notes, however, that $V7$ is a semi-regular variable, so that its suspected variability at 12 μm must be of a different nature than that of oxygen-rich Miras (see Section 3 for further discussion).

2.2. DENIS K_s Image

The K_s magnitudes of the sources detected on the ISOCAM image at 12 μm have been obtained from aperture photometry on the DENIS image of the same field. The DENIS raw K_s magnitudes have been converted into Frogel et al. (1981) system of K magnitudes. The transformation equation has been derived from the four bright variables $V7, V11, V15$ and $V18$ common to the two samples (although they are among the brightest stars in the cluster, they may be expected to be constant at the level of 0.1 mag in the K band, since they vary by less than 0.9 mag in V; Lloyd Evans 1974, Fox 1982). In order to extend the calibration to fainter objects, K magnitudes in Frogel's system have been estimated for several stars on the DENIS images having UBV data from Lee (1977). These stars are first assigned to either the RGB, AGB or GB (where the RGB and AGB merge) from their location in the $(U - B, B - V)$ diagram of Lee (1977). The adopted K magnitude is then that of a star with a similar $B - V$ index and RGB, AGB or GB assignment in the sample of Frogel et al. (1981). The above method yields the transformation equation $K = 0.89(\pm 0.02)K_s + 17.97(\pm 0.21)$.

The standard deviation of the $K(\mathrm{DENIS}) - K(\mathrm{Frogel})$ differences is 0.14 mag, which gives an indication of the overall accuracy of the transformation.

2.3. *Digital Sky Survey* V Image

The V image was obtained from the *Digital Sky Survey*. Figure 2 identifies the 12 μm sources on the visible image. Basically all sources brighter than $V = 14$ (i.e. $M_V < -0.9$ for the distance modulus $V - M_V = 13.1$ of 47 Tuc) are detected at 12 μm, corresponding to a detection threshold of about 0.7 mJy, allowing to detect all the giants down to almost the horizontal branch.

A few sources with no optical counterparts are visible on Figure 2. Their 12 μm flux covers the range 0.4 – 1.6 mJy, to be compared with 50 – 200 mJy for the

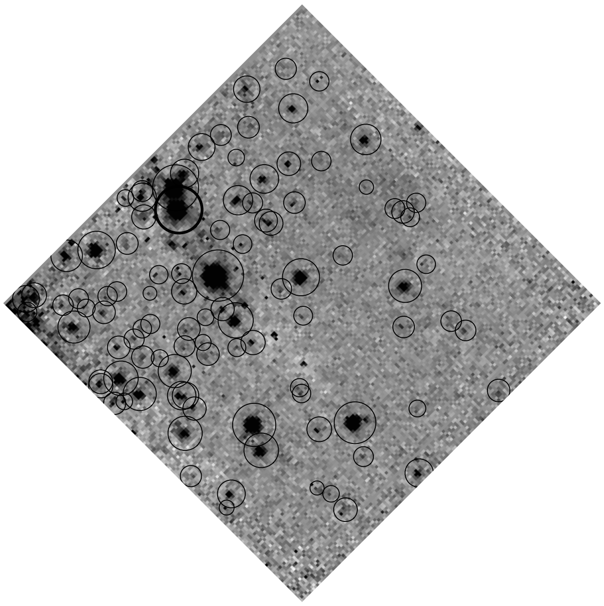

Figure 1. The ISOCAM 12 μm image, with the same orientation as the optical image (Fig. 2). The variable V18 discussed in the text is identified by the thick circle.

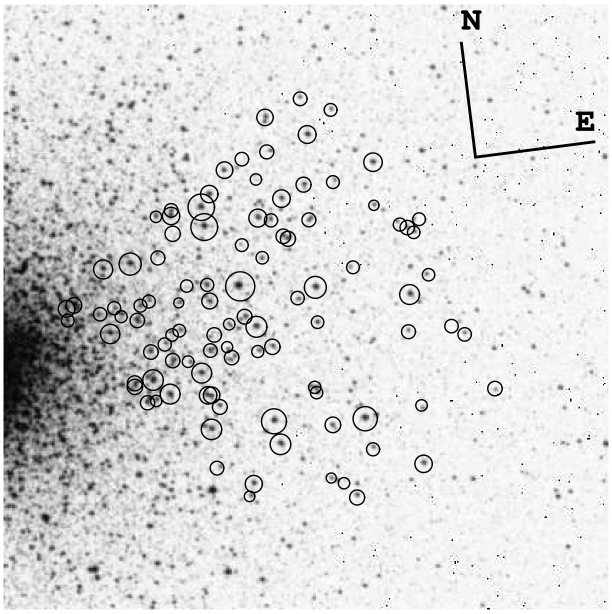

Figure 2. The Digital Sky Survey 12′ × 12′ image of the ISOCAM field, with 12 μm sources identified by circles with a radius proportional to their 12 μm flux.

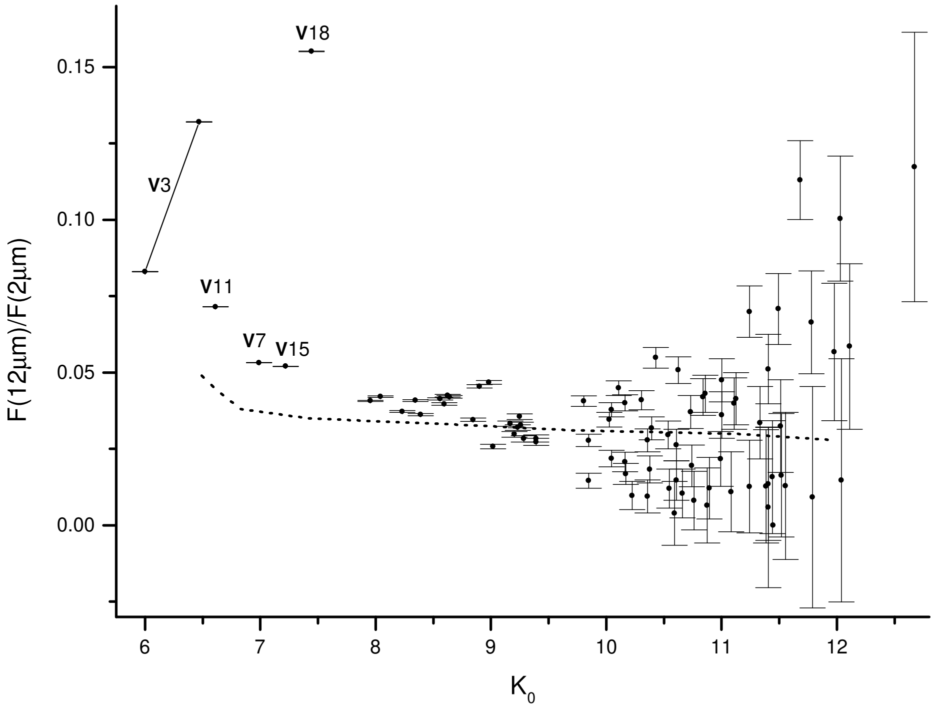

Figure 3. The F12/F2 vs K diagram for stars detected at 2 and 12 μm, with the variable stars identified. The conversion from K magnitudes to fluxes was performed by adopting a zero-magnitude flux of 620 Jy, following Beckwith et al. (1976). Note that the distance modulus of 47 Tuc is 13.1. The oblique segment for V3 translates its variability in the K band only (see Table 2), as existing data do not allow yet to estimate its variability range at 12 μm. The dashed line represents black body colors (see text).

brightest AGB variables (Table 2). As these sources neither have a K counterpart nor are as bright as would be expected for obscured AGB stars emitting only in the IR (e.g. Tanabé et al. 1997), their reality still needs to be confirmed from a careful re-analysis of the raw 12 μm data; they might be ghost images caused by internal reflections within the camera of the bright sources present in our field (ISOCAM manual v.1, Sect. 2.1; Okumura et al. 1998).

Conversely, the absence of IR-bright, optically-obscured sources in this field is in itself an interesting result which may be used to derive constraints on the lifetime of obscured AGB stars of low-mass and metallicity.

3. THE $F12/F2$ MASS LOSS INDEX

The ratio $F12/F2$ of the 12 to 2 μm flux densities is expected to be a good indicator of mass loss (see Habing 1996 and references therein; Le Bertre & Winters 1998).

Figure 3 presents the $F_\nu(12\mu\text{m})/F_\nu(2\mu\text{m})$ vs. K diagram for all the sources detected at 2 and 12 μm. The error bars reflect the uncertainty on the adopted background value around the source and the Poissonian noise on the signal. For comparison, the trend expected for black bodies of different temperatures is represented by the dashed line. The relation between temperatures and K magnitudes along the giant branch of 47 Tuc is derived from Tables 4 and 6 of Frogel et al. (1981). The $F12/F2$ ratio at the faint end of the K distribution ($K > 8$, corresponding to $T > 3800$ K) is roughly constant, since the K and 12 μm filters then fall in the Rayleigh-Jeans (RJ) tail of the spectrum. It should be mentioned that the black body ratio has been multiplied by the factor 0.45 so as to fit the observed RJ value of ~ 0.025. Until the origin of this discrepancy is properly understood (and especially until the impact on the estimated ISO fluxes of the adopted photometric calibration factor, of the undue masking of bright pixels by the multi-median deglitching routine, of PSF, transient and colour corrections has been properly assessed; Blommaert 1998), the ISO fluxes listed in the present paper should be considered as preliminary.

Figure 3 clearly shows that no significant deviations from the black body line representing the photospheric colors arise for the warm and low-luminosity giants having $K > 8$ ($M_K > -5$ for a distance modulus of 13). Therefore, it may be concluded that *stars with a clean circumstellar environment (hence suffering from a mass loss low enough not to produce a dust shell visible at 12 μm) populate the giant branch up to about $M_K = -5$ in the low-metallicity environment of 47 Tuc.*

All brighter stars are variable (see Fox 1982 for a description of their light curves and periods, and Fig. 1 of Frogel et al. 1981 for their location in the Hertzsprung-Russell diagram), and some have $F12/F2$ ratios well in excess of 0.05 indicative of a dust shell. Among the variables displayed on Fig. 3, only $V3$ is a Mira (with a period of 192 d). The even larger 12 μm excess observed for $V18$ is surprising, especially when compared to the absence of a similar excess for the stars $V7, V11$ and $V15$, which are located slightly above $V18$ on the giant branch.

The origin of the difference between the $F12/F2$ ratios of variable stars of comparable luminosities must therefore be searched for in their variability properties. Arguments indicating that the 12 μm flux of oxygen-rich *Mira* variables may vary by a factor of 2 were already presented in Section 2.1. This argument does not apply to $V18$, however, since it is not a Mira variable. Interestingly enough, Fox (1982) notes that $V18$ may be of the type of variable that switches on and off intermittently. It is tempting to relate this behaviour with the sudden ejection of dust shells causing the star to brighten up at 12 μm. A similar phenomenon has been proposed for semi-regular variable stars by Ivezić & Knapp (1999).

In any case, the present conclusions reinforce the connection between stellar variability and the mass loss process (e.g. Frogel & Elias 1988, Habing 1996 and references therein).

ACKNOWLEDGMENTS

D. Elbaz and H. Aussel are thanked for their help with the reduction of the data.

REFERENCES

Aussel H., Cesarsky C.J., Elbaz D., Starck J.L., 1998, A&A, in press (astro-ph/9810044)

Beckwith S., Evans N.J., Becklin E.E., Neugebauer G., 1976, ApJ 208, 390

Blommaert J., 1998, ISOCAM photometry report v. 2.1 (available at http://www.iso.vilspa.esa.es/users/expl_lib/CAM_list.html)

Fox M.W., 1982, MNRAS 199, 715

Frogel J.A., Persson S.E., Cohen J.G., 1981, ApJ 246, 842

Frogel J.A., Elias J.H., 1988, ApJ 324, 823

Gillett F.C., de Jong T., Neugebauer G., Rice W.L., Emerson J.P., 1988, AJ 96, 116

Habing H.J., 1996, A&A Rev. 7, 97

Ivezić Ž., Knapp G.R., 1999, in: AGB Stars (IAU Symp. 191), T. Le Bertre, A. Lèbre, C. Waelkens (eds.) ASP Conf. Ser., in press

Jorissen A., Knapp G.R., 1998, A&AS 129, 363

Lee S.-W., 1977, A&AS 27, 381

Le Bertre T., 1993, A&AS 97, 729

Le Bertre T., Winters J.M., 1998, A&A 334, 173

Lloyd Evans T., 1974, MNRAS 167, 393

Okumura K., Pérault M., Longval Y., 1998, Ghosts in ISOCAM images (available at http://www.iso.vilspa.esa.es/users/expl_lib/CAM_list.html)

Starck J.L., Aussel H., Elbaz D., et al., 1998, in: Extragalactic Astronomy in the Infrared, Mamon G.A., Thuan T.X., Tran Thanh Van J. (eds.) Editions Frontières, p. 509

Tanabé T., Nishida S., Matsumoto S., et al., 1997, Nature 385, 509